



# Loss of insulin signaling may contribute to atrial fibrillation and atrial electrical remodeling in type 1 diabetes

Iuliia Polina<sup>a,1</sup>, Hailey J. Jansen<sup>a,b,c,1</sup>, Tiesong Li<sup>a</sup>, Motahareh Moghtadaei<sup>a,b,c</sup>, Loryn J. Bohne<sup>b,c</sup>, Yingjie Liu<sup>b,c</sup>, Pooja Krishnaswamy<sup>a</sup>, Emmanuel E. Egom<sup>a</sup>, Darrell D. Belke<sup>b,c</sup>, Sara A. Rafferty<sup>a</sup>, Martin Ezeani<sup>a</sup>, Anne M. Gillis<sup>b,c</sup>, and Robert A. Rose<sup>a,b,c,2</sup>

<sup>a</sup>Department of Physiology and Biophysics, Faculty of Medicine, Dalhousie University, Halifax, NS, Canada, B3H 4R2; <sup>b</sup>Libin Cardiovascular Institute of Alberta, Department of Cardiac Sciences, Cumming School of Medicine, University of Calgary, Calgary, AB, Canada, T2N 4Z6; and <sup>c</sup>Libin Cardiovascular Institute of Alberta, Department of Physiology and Pharmacology, Cumming School of Medicine, University of Calgary, Calgary, AB, Canada, T2N 4Z6

Edited by Christine E. Seidman, Howard Hughes Medical Institute, Brigham and Women's Hospital and Harvard Medical School, Boston, MA, and approved February 20, 2020 (received for review August 29, 2019)

**Atrial fibrillation (AF) is prevalent in diabetes mellitus (DM); however, the basis for this is unknown. This study investigated AF susceptibility and atrial electrophysiology in type 1 diabetic Akita mice using in vivo intracardiac electrophysiology, high-resolution optical mapping in atrial preparations, and patch clamping in isolated atrial myocytes. qPCR and western blotting were used to assess ion channel expression. Akita mice were highly susceptible to AF in association with increased P-wave duration and slowed atrial conduction velocity. In a second model of type 1 DM, mice treated with streptozotocin (STZ) showed a similar increase in susceptibility to AF. Chronic insulin treatment reduced susceptibility and duration of AF and shortened P-wave duration in Akita mice. Atrial action potential (AP) morphology was altered in Akita mice due to a reduction in upstroke velocity and increases in AP duration. In Akita mice, atrial Na<sup>+</sup> current (I<sub>Na</sub>) and repolarizing K<sup>+</sup> current (I<sub>K</sub>) carried by voltage gated K<sup>+</sup> (K<sub>v</sub>1.5) channels were reduced. The reduction in I<sub>Na</sub> occurred in association with reduced expression of *SCN5a* and voltage gated Na<sup>+</sup> (Na<sub>v</sub>1.5) channels as well as a shift in I<sub>Na</sub> activation kinetics. Insulin potently and selectively increased I<sub>Na</sub> in Akita mice without affecting I<sub>K</sub>. Chronic insulin treatment increased I<sub>Na</sub> in association with increased expression of Na<sub>v</sub>1.5. Acute insulin also increased I<sub>Na</sub>, although to a smaller extent, due to enhanced insulin signaling via phosphatidylinositol 3,4,5-triphosphate (PIP<sub>3</sub>). Our study reveals a critical, selective role for insulin in regulating atrial I<sub>Na</sub>, which impacts susceptibility to AF in type 1 DM.**

atrial fibrillation | diabetes mellitus | phosphoinositide 3-kinase | action potential | Na<sup>+</sup> current

**A**trial fibrillation (AF), the most common sustained arrhythmia encountered clinically (1, 2), is highly prevalent in diabetes mellitus (DM) (3–6). AF increases the risk of stroke and death and has a substantial negative impact on quality of life. While AF and DM share some common risk factors, it is also clear that DM is an independent risk factor for the development of AF (7, 8). Consistent with this, a longer duration of untreated DM or poor glycemic control independently and significantly increases the risk of developing AF (5, 9). Furthermore, AF is clearly associated with a worse prognosis in diabetic patients, greatly increasing the risk of adverse cardiovascular events and all-cause mortality (3, 6). Despite these links, the mechanisms leading to a substrate for AF in DM are not understood, which likely contributes to the limited efficacy of current AF therapies.

Type 1 DM, which affects up to 10% of the global diabetic population (10), is characterized by a lack of insulin production due to the loss of pancreatic  $\beta$  cells that results in hypoinsulinemia and hyperglycemia. Under normal conditions, insulin binds to its receptor and activates the phospho-

inositide 3-kinase (PI3K) pathway (11, 12). Specifically, insulin activates PI3K $\alpha$ , which phosphorylates phosphatidylinositol 4,5-bisphosphate (PIP<sub>2</sub>) to produce the second messenger phosphatidylinositol 3,4,5-triphosphate (PIP<sub>3</sub>). PIP<sub>3</sub> mediates many key effects of insulin, including in the heart (13, 14).

Electrical remodeling in the atria is known to be an important contributor to the creation of a substrate for AF (15, 16). At the cellular level, atrial action potential (AP) morphology is a major determinant of atrial electrophysiology. The upstroke velocity of the AP is determined by the Na<sup>+</sup> current (I<sub>Na</sub>), which is a major contributor to atrial conduction velocity (17, 18). Cardiac I<sub>Na</sub> is primarily carried by voltage gated Na<sup>+</sup> channels (Na<sub>v</sub>1.5), which are encoded by the *SCN5a* gene. Alterations in atrial I<sub>Na</sub> and AP upstroke velocity can affect atrial conduction velocity and the likelihood of electrical reentry, thereby affecting susceptibility to AF (2, 15). Action potential duration (APD) and repolarization of the AP are affected by the balance between several inward and outward currents, including the L-type Ca<sup>2+</sup> current (I<sub>Ca,L</sub>) and the late Na<sup>+</sup> current (I<sub>Na,L</sub>), and the activity of a number of voltage gated K<sup>+</sup> (K<sub>v</sub>) channels, including, among others, the transient outward K<sup>+</sup> current (I<sub>to</sub>; carried by K<sub>v</sub>4.2/4.3 channels)

## Significance

**Atrial fibrillation (AF) is prevalent in diabetic patients, yet the basis for AF in diabetes is poorly understood. We have used type 1 diabetic Akita mice to study the effects of insulin on atrial electrophysiology in diabetes. We demonstrate that Akita mice are highly susceptible to AF due to impaired electrical conduction and that insulin treatment can reduce the occurrence of this arrhythmia. Atrial action potential morphology was altered in Akita mice in association with reductions in atrial Na<sup>+</sup> current (I<sub>Na</sub>) and repolarizing potassium current. Insulin treatment potently increased atrial I<sub>Na</sub> via distinct chronic and acute effects. These experiments identify antiarrhythmic effects of insulin in type 1 diabetes via potent effects on atrial I<sub>Na</sub>.**

Author contributions: I.P., H.J.J., and R.A.R. designed research; I.P., H.J.J., T.L., M.M., L.J.B., Y.L., P.K., E.E.E., D.D.B., S.A.R., M.E., and R.A.R. performed research; I.P., H.J.J., T.L., M.M., L.J.B., Y.L., D.D.B., A.M.G., and R.A.R. analyzed data; and I.P., H.J.J., A.M.G., and R.A.R. wrote the paper.

The authors declare no competing interest.

This article is a PNAS Direct Submission.

Published under the [PNAS license](#).

<sup>1</sup>I.P. and H.J.J. contributed equally to this work.

<sup>2</sup>To whom correspondence may be addressed. Email: robert.rose@ucalgary.ca.

This article contains supporting information online at <https://www.pnas.org/lookup/suppl/doi:10.1073/pnas.1914853117/-DCSupplemental>.

First published March 20, 2020.

and the ultrarapid delayed rectifier  $K^+$  current ( $I_{Kur}$ ; an atrial-specific current carried by  $K_{V1.5}$  channels).

The goal of the present study was to investigate atrial electrophysiology and the basis for AF in type 1 DM. Our studies were conducted using the Akita mouse model of type 1 DM as well as wild-type mice injected with streptozotocin (STZ) (19, 20). Each of these is a well-validated model of type 1 DM (19). Our data demonstrate that Akita and STZ-injected mice are highly susceptible to induced AF. Furthermore, AF inducibility is reduced by insulin treatment in Akita mice. Our mechanistic studies show that AF in Akita mice is associated with alterations in atrial AP morphology and that insulin has distinct acute and chronic effects on AP morphology and  $I_{Na}$  in the atria.

## Results

**Susceptibility to AF in Type 1 Diabetic Mice.** Burst pacing was used to assess susceptibility to AF (Fig. 1A) in anesthetized wild-type and Akita mice. Blood glucose was elevated in Akita mice compared with wild types (SI Appendix, Fig. S1A). Strikingly, Akita mice were highly susceptible to induced AF compared with wild-type mice (Fig. 1B). The episodes of AF induced in two wild-type mice were very brief, lasting less than 5 s (Fig. 1C). In contrast, AF induced in Akita mice was longer in duration. Specifically, 62% of the Akita mice had AF between 5 and 30 s, and 23% of Akita mice were induced into AF lasting longer than 30 s (Fig. 1C and SI Appendix, Table S1). To ensure that these observations were not specific to the Akita model of type 1 DM, we also investigated AF susceptibility in a second model of type 1 DM secondary to STZ injection in wild-type mice. STZ injection led to hyperglycemia as indicated by increases in blood glucose (SI Appendix, Fig. S2A). Furthermore, STZ-injected mice displayed similar increases in AF inducibility (SI Appendix, Fig. S2B and C) and AF duration (SI Appendix, Fig. S2D and Table S2) to Akita

mice. Together, these data illustrate that both mouse models of type 1 DM display increased susceptibility to AF.

Next, we assessed the effects of chronic insulin treatment on AF burden in Akita mice. Insulin pellet implantation reduced blood glucose levels in Akita mice to levels that were similar to wild types, while placebo pellets had no effect on blood glucose in Akita mice (SI Appendix, Fig. S1B). Following chronic insulin treatment, only 25% of Akita mice were induced into AF compared with 62% of placebo-treated Akita mice (Fig. 1D). In addition, when AF was induced in insulin-treated Akita mice, the episodes were brief, lasting less than 5 s in 83% of the mice. No insulin-treated Akita mice had AF lasting longer than 30 s (Fig. 1E and SI Appendix, Table S3). In contrast, 50% of placebo-treated Akita mice demonstrated AF lasting longer than 5 s, and in some cases, it lasted longer than 30 s (Fig. 1E and SI Appendix, Table S3). These data demonstrate that chronic insulin treatment reduced both the susceptibility and the duration of AF in Akita mice.

We also examined the effects of acute insulin treatment on AF in Akita mice. Acute intraperitoneal injection of insulin (5 to 10 U/kg) reduced blood glucose in Akita mice to values similar to wild-type mice within 30 to 45 min, while saline-injected Akita mice were unaffected (SI Appendix, Fig. S1C). Acute insulin injection had no effect on inducibility of AF in Akita mice (Fig. 1F and SI Appendix, Table S4); however, the median AF duration was lower in Akita mice following acute insulin treatment (Fig. 1G).

**Atrial Electrophysiology in Type 1 Diabetic Mice.** P-wave duration and P wave–R wave (PR) intervals were assessed in Akita mice and STZ-treated mice. Compared with wild types, Akita mice had prolonged P-wave duration (Fig. 2A–C) and PR intervals (SI Appendix, Table S5). P-wave duration and PR interval were also

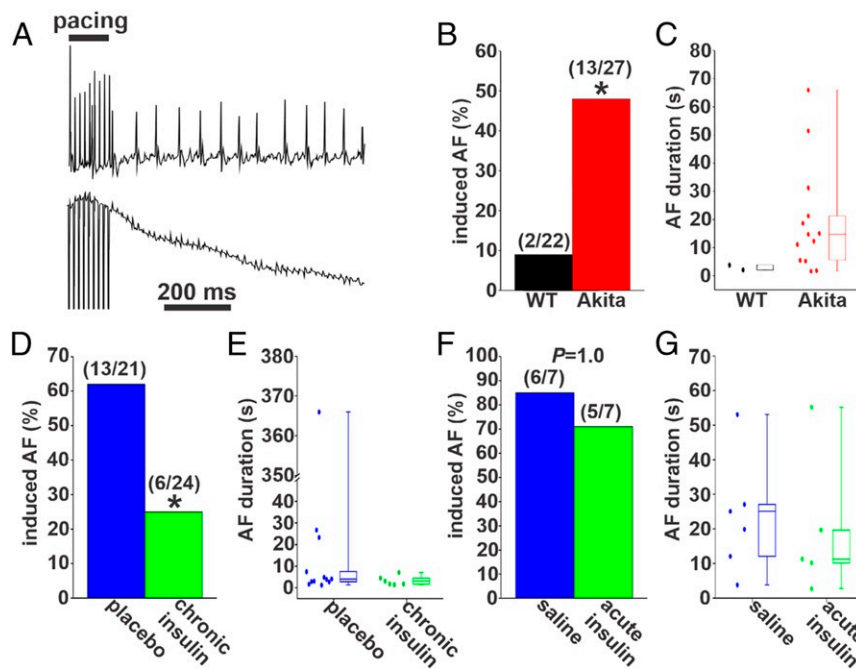


**Fig. 1.** AF in untreated Akita mice and Akita mice treated with insulin. (A) Representative surface (Upper) and intracardiac atrial (Lower) ECGs showing the induction of AF in an untreated anesthetized Akita mouse following burst pacing. (B) Inducibility of AF in untreated wild-type (WT) and Akita mice. Numbers in parentheses indicate the number of mice induced into AF following burst pacing. \* $P < 0.05$  by Fisher's exact test. (C) Duration of AF in the WT ( $n = 2$ ) and Akita ( $n = 13$ ) mice that were induced into AF. (D) Inducibility of AF in Akita mice treated chronically with insulin or placebo for 4 wk. \* $P < 0.05$  vs. placebo by Fisher's exact test. (E) Duration of AF in the placebo- ( $n = 13$ ) and insulin-treated ( $n = 6$ ) Akita mice that were induced into AF. (F) Inducibility of AF in Akita mice treated acutely with insulin or saline. Data were analyzed by Fisher's exact test. (G) Summary data demonstrating the duration of AF in the saline- ( $n = 7$ ) and insulin-treated ( $n = 5$ ) Akita mice that were induced into AF. SI Appendix, Tables S1–S4 have additional AF analysis.

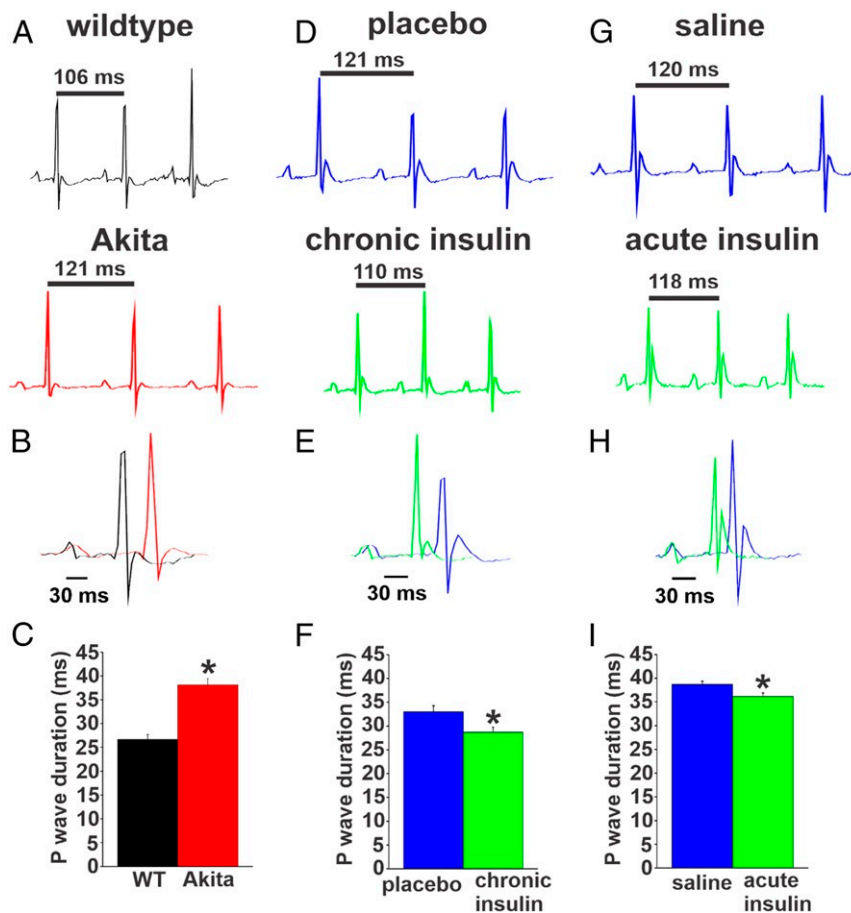


**Fig. 2.** P-wave duration in untreated Akita mice and Akita mice treated with insulin. (A) Representative surface ECGs from untreated wild-type (WT) and Akita mice. (B) Overlay of ECGs from WT and Akita mice. (C) Summary of P-wave duration in untreated WT and Akita mice.  $n = 7$  WT mice and 10 Akita mice.  $*P < 0.05$  vs. WT by Student's  $t$  test. (D) Representative surface ECGs from Akita mice treated chronically with insulin or placebo pellets for 4 wk. (E) Overlay of ECGs from Akita mice treated chronically with insulin or placebo pellets. (F) Summary of the effects of chronic insulin on P-wave duration in Akita mice.  $n = 21$  placebo-treated mice and 22 insulin-treated mice.  $*P < 0.05$  vs. placebo by Student's  $t$  test. (G) Representative surface ECGs from Akita mice treated acutely with insulin or saline by intraperitoneal injection. (H) Overlay of ECGs from Akita mice treated acutely with insulin. (I) Summary of the effects of acute insulin treatment on P-wave duration in Akita mice.  $n = 8$  saline-treated mice and 7 insulin-treated mice. *SI Appendix, Tables S5–S8* has additional ECG analysis.  $*P < 0.05$  vs. placebo by Student's  $t$  test.

prolonged in STZ-treated mice (*SI Appendix, Fig. S2 E and F and Table S6*). Chronic insulin treatment shortened P-wave duration (Fig. 2 D–F) and tended to reduce the PR interval in Akita mice compared with placebo controls (*SI Appendix, Table S7*). Acute insulin treatment also shortened P-wave duration in Akita mice (Fig. 2 G–I), although this effect was smaller in magnitude compared with chronic insulin treatment. These findings indicate that atrial conduction is impaired in type 1 diabetic mice and improved following chronic as well as acute insulin treatment.

Patterns of atrial conduction in Akita mice were assessed using high-resolution optical mapping in isolated atrial preparations from wild-type and Akita mice. Representative activation maps (Fig. 3A) illustrate that conduction initiates in the right atrial posterior wall and then spreads across the full atrial preparation (21–23). These representative maps show that total conduction time across the full atrial preparation is longer in Akita mice. We also quantified local conduction velocities within the right and left atrial appendage regions. Right and left atrial conduction velocities were both reduced in Akita mice compared with the wild types (Fig. 3B), further confirming that atrial conduction is impaired in Akita mice. Consistent with the changes in P-wave duration measured *in vivo*, optical mapping studies also demonstrate that chronic insulin treatment in Akita mice resulted in

faster conduction time across the atria (Fig. 3C) and increased right and left atrial conduction velocities (Fig. 3D).

Echocardiographic assessment (*SI Appendix, Fig. S3 and Table S9*) demonstrates that Akita mice did not display substantial changes in ventricular structure or function, which is consistent with prior studies (24). Although maximum left atrial area was modestly increased in Akita mice, other measures of atrial size were similar between wild-type and Akita mice (*SI Appendix, Fig. S3 and Table S9*). Serum  $[Na^+]$  and  $[Cl^-]$  were modestly reduced, while serum  $[K^+]$  and  $[Ca^{2+}]$  were not altered in Akita mice compared with wild-type controls (*SI Appendix, Fig. S4*).

**Alterations in Atrial Myocyte Electrophysiology in Akita Mice.** To further investigate the basis for increased AF and impaired atrial conduction in Akita mice, we measured APs in isolated right and left atrial myocytes (Fig. 4A and B). Consistent with the absence of major changes in atrial size, there were no differences in cell capacitance in right atrial myocytes ( $50.6 \pm 5.1$  vs.  $52.9 \pm 7.3$  pF;  $P = 0.84$ ) or left atrial myocytes ( $54 \pm 4.1$  vs.  $58.8 \pm 5.8$  pF;  $P = 0.50$ ) between wild-type and Akita mice, indicating no differences in cell size. AP upstroke velocity (maximum upstroke velocity  $[V_{max}]$ ) was reduced in right and left atrial myocytes from Akita mice compared with wild-type controls (Fig. 4C and D). Furthermore, APD was prolonged throughout repolarization



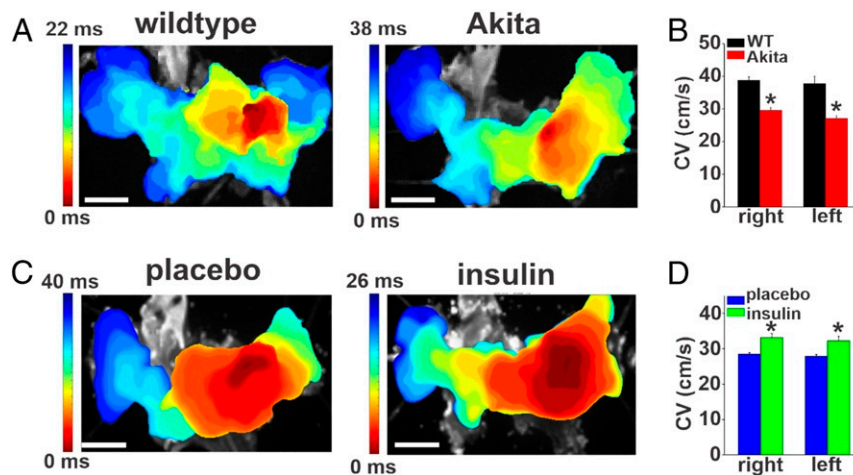


**Fig. 3.** Patterns of electrical conduction in the atria in untreated Akita mice and Akita mice treated chronically with insulin. (A) Representative activation maps in isolated atrial preparations from wild-type (WT) and untreated Akita mice. The right atrial appendage is on the right side of the image. Red indicates the earliest activation time. The color scale indicates total conduction time across the atrial preparation. (Scale bar: 3 mm.) (B) Summary of local right and left atrial conduction velocities (CV) (SI Appendix, Supplemental Methods) in WT and Akita mice.  $n = 7$  WT and 8 Akita hearts. \* $P < 0.05$  vs. WT by two-way ANOVA with Tukey's post hoc test. (C) Representative activation maps in atrial preparations from Akita mice treated with placebo or chronically with insulin for 4 wk. (D) Summary of local right and left atrial conduction velocities in placebo- and insulin-treated Akita mice.  $n = 6$  placebo- and 5 insulin-treated Akita hearts. \* $P < 0.05$  vs. placebo by two-way ANOVA with Tukey's post hoc test.

in both right and left atrial myocytes from Akita mice (Fig. 4 E and F). These alterations in AP morphology occurred without changes in resting membrane potential (SI Appendix, Tables S10 and S11).

To ensure that the changes in APD observed in isolated cells were not a consequence of cell isolation procedures, we also measured APDs in wild-type and Akita mice using optical mapping (SI Appendix, Fig. S5). Optical APs measured in the right and left atria of intact atrial preparations confirm that APD was prolonged in Akita mice (SI Appendix, Fig. S5).

AP morphology was also assessed in isolated ventricular myocytes from wild-type and Akita mice (SI Appendix, Fig. S6 and Table S12). APD was prolonged in Akita ventricular myocytes; however, in contrast to atrial myocytes, there were no differences in AP  $V_{max}$  in Akita ventricular myocytes.

The alterations in atrial conduction (prolonged P-wave duration, reduced atrial conduction velocity) as well as the reduction in atrial AP  $V_{max}$  in Akita mice are suggestive of changes in atrial  $I_{Na}$ . Accordingly, we measured  $I_{Na}$  in isolated right and left atrial myocytes from wild-type and Akita mice (Fig. 5A and SI Appendix, Fig. S7). Summary current–voltage (IV) curves for right atrial myocytes demonstrate that  $I_{Na}$  is reduced in Akita mice (Fig. 5B).  $I_{Na}$  activation curves (Fig. 5C) and analysis of  $I_{Na}$  activation kinetics (SI Appendix, Table S13) demonstrate that the reduction in  $I_{Na}$  density in Akita mice occurred in association with a reduction in maximum conductance ( $G_{max}$ ) and a modest (~3-mV) rightward shift in the voltage dependence of activation [ $V_{1/2(act)}$ ]. Similar alterations in  $I_{Na}$  density,  $G_{max}$ , and activation kinetics were observed in left atrial myocytes from Akita mice (SI Appendix, Fig. S7 and Table S13). We also measured steady-state inactivation in right atrial myocytes in Akita mice (SI Appendix, Fig. S8). Voltage dependence of inactivation was not altered in Akita right atrial myocytes.

Because the reductions in  $I_{Na}$  density and  $G_{max}$  were large relative to the shift in  $V_{1/2(act)}$ , we also measured the expression of *SCN5a* messenger ribonucleic acid (mRNA) as well as Nav1.5 protein in the atria of wild-type and Akita mice. These data show that expressions of *SCN5a* (Fig. 5D and SI Appendix, Fig. S7D) and Nav1.5 (Fig. 5E and SI Appendix, Fig. S7E) were reduced in the right and left atria of Akita mice compared with wild-type controls.

Next, we investigated the properties and expression of repolarizing  $K^+$  current ( $I_K$ ) in order to assess the ionic basis for the prolongation in atrial APD observed in Akita mice. We first measured  $I_K$  in right atrial myocytes from wild-type and Akita mice.  $I_K$  was measured with and without a prepulse to inactivate  $I_{to}$  (25, 26) (Fig. 6A and SI Appendix, Supplemental Methods). Summary  $I_K$  IV relationships illustrate that peak total (i.e., no prepulse)  $I_K$  was reduced in Akita mice at membrane potentials positive to +20 mV (Fig. 6B). Consistent with the lack of differences in resting membrane potential, there were no differences in  $I_K$  in the region of the IV curves where inward rectifier  $K^+$  current ( $I_{K1}$ ) is active (i.e., negative to –80 mV) between wild-type and Akita mice. IV curves for peak  $I_K$  measured from the protocols with an inactivating prepulse demonstrate that  $I_K$  remained reduced in Akita mice at membrane potentials positive to +20 mV (Fig. 6C) when  $I_{to}$  is inactivated. In agreement with these observations, IV relationships for  $I_{to}$  (i.e., the difference current between measurements with and without the inactivating prepulse) illustrate no differences between wild-type and Akita mice (Fig. 6D). Very similar observations were made for  $I_K$  in left atrial myocytes from wild-type and Akita mice (SI Appendix, Fig. S9). Further evidence that the reduction in repolarizing  $I_K$  in Akita mice does not involve  $I_{to}$  was obtained from western blot studies, which show no differences in the protein levels of  $K_v4.2$  and  $K_v4.3$  in right and left atria from wild-type and Akita mice (SI Appendix, Fig. S10).

The  $I_{Kur}$  carried by  $K_v1.5$  channels was investigated by measuring the component of  $I_K$  sensitive to 4-aminopyridine (4-AP) (100  $\mu$ M) (Fig. 6E) (26, 27) in right atrial myocytes from wild-type and Akita mice. From these representative recordings, it is apparent that outward  $I_K$  is smaller at baseline and that the reduction in  $I_K$  elicited by 4-AP was smaller in Akita mice. These recordings also demonstrate that the effects of 4-AP were reversible on washout. Summary data confirm that the 4-AP-sensitive current (i.e.,  $K_v1.5$ -mediated  $I_{Kur}$ ) is reduced in Akita mice (Fig. 6F). The expression of the *KCNA5* gene (which encodes  $K_v1.5$ ) was not different in Akita mice (SI Appendix, Fig. S11A); however, in agreement with the reduction in current,  $K_v1.5$  protein in Akita right atrium was reduced compared with wild-type controls (SI Appendix, Fig. S11B).

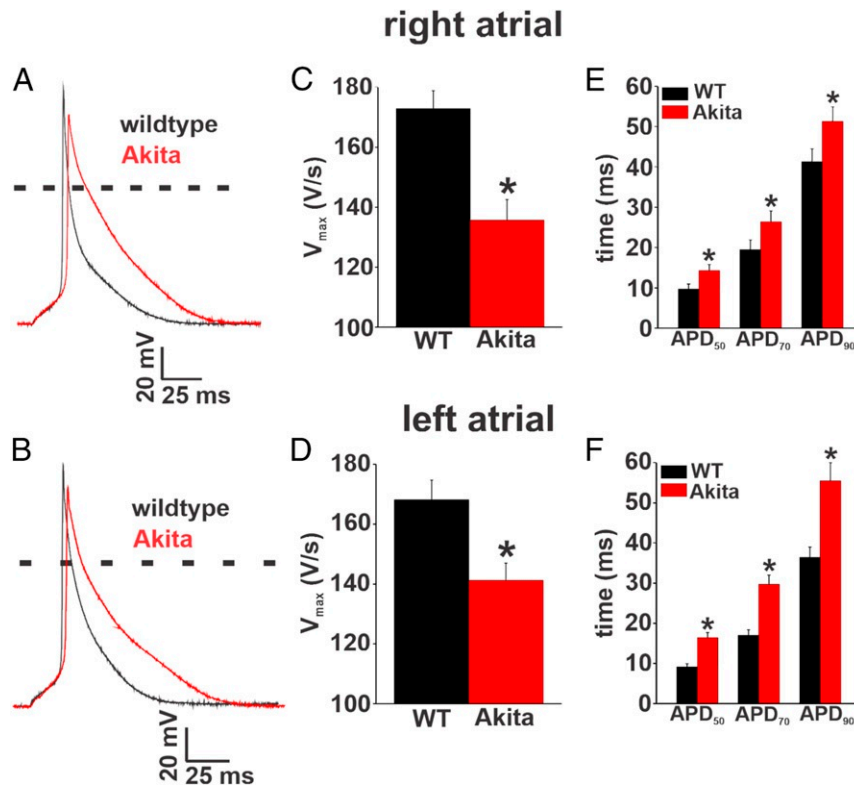


**Fig. 4.** Right and left atrial AP morphology in Akita mice. (A and B) Representative stimulated APs in isolated right atrial (A) and left atrial (B) myocytes from wild-type (WT) and Akita mice. (C and D) Summary of AP  $V_{max}$  in isolated right atrial (C) and left atrial (D) myocytes from WT and Akita mice. (E and F) Summary of APD in isolated right atrial (E) and left atrial (F) myocytes from WT and Akita mice. APD was measured at 50% (APD<sub>50</sub>), 70% (APD<sub>70</sub>), and 90% (APD<sub>90</sub>) repolarization. For right atrial myocytes,  $n = 18$  for the WT and 16 for Akita. For left atrial myocytes,  $n = 12$  for the WT and 11 for Akita. *SI Appendix, Tables S10 and S11* has additional AP analysis. \* $P < 0.05$  vs. the WT by Student's  $t$  test.

APD can also be affected by other currents, such as  $I_{Ca,L}$  and  $I_{Na,L}$ , which were both assessed in Akita right atrial myocytes.  $I_{Ca,L}$  (*SI Appendix, Fig. S12*) and  $I_{Na,L}$  (*SI Appendix, Fig. S13*)

were not different between wild-type and Akita mice. There were also no differences in atrial calcium transient morphology between wild-type and Akita mice (*SI Appendix, Fig. S14*). As

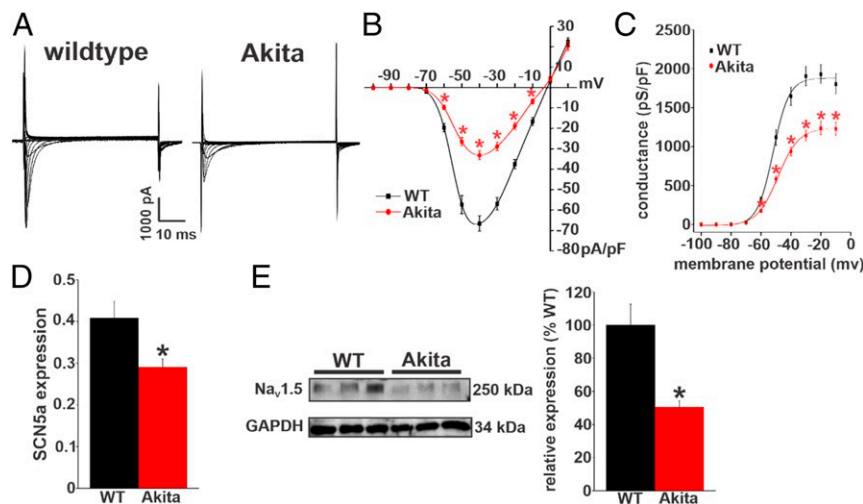


**Fig. 5.**  $I_{Na}$  is reduced in right atrial myocytes in Akita mice. (A) Representative  $I_{Na}$  recordings in right atrial myocytes isolated from wild-type (WT) and Akita mice. Cell capacitance for these representative recordings was 44 pF for the WT and 41 pF for Akita. (B)  $I_{Na}$  IV curves in right atrial myocytes isolated from WT and Akita mice. Current densities are measured in picoamperes/picofarad (pA/pF). (C) Summary  $I_{Na}$  activation curves in right atrial myocytes from WT and Akita mice. Conductance is measured in picosiemens/picofarad (pS/pF);  $n = 21$  myocytes for the WT and 18 for Akita.  $I_{Na}$  activation kinetics are summarized in *SI Appendix, Table S13*. \* $P < 0.05$  vs. the WT at each membrane potential by two-way repeated measures ANOVA with Tukey's post hoc test. (D)  $SCN5a$  mRNA expression in the right atrium in WT and Akita mice.  $n = 23$  WT and 15 Akita mice. \* $P < 0.05$  vs. the WT by Student's  $t$  test. (E)  $Na_V1.5$  protein expression in the right atrium in WT and Akita mice.  $n = 6$  WT and 6 Akita mice. \* $P < 0.05$  vs. the WT by Student's  $t$  test.

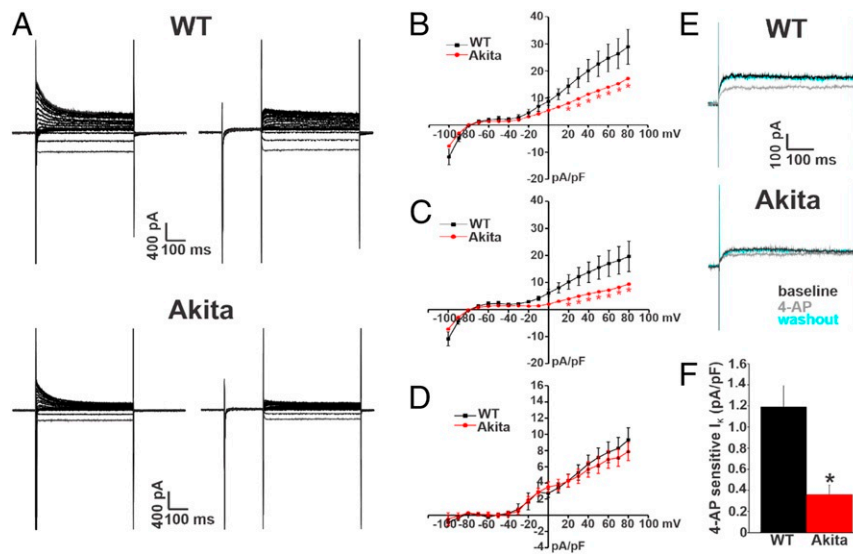


**Fig. 6.** Repolarizing  $I_K$  is reduced in right atrial myocytes in Akita mice. (A) Representative  $I_K$  recordings in right atrial myocytes isolated from wild-type (WT) and Akita mice. The recordings on the left represent total  $I_K$  measured between  $-100$  and  $+80$  mV. The recordings on the right represent  $I_K$  measured between  $-100$  and  $+80$  mV following a prepulse to  $-40$  mV to inactivate  $I_{to}$ . Cell capacitances for these representative recordings were  $33$  pF for the WT and  $38$  pF for Akita. (B) Summary  $I_K$  IV curves measured at the peak of the  $I_K$  recordings without the prepulse (recordings on the left in A) for right atrial myocytes isolated from WT and Akita mice. (C) Summary  $I_K$  IV curves measured at the peak of the  $I_K$  recordings with the prepulse (recordings on the right in A) for right atrial myocytes isolated from WT and Akita mice. \* $P < 0.05$  vs. the WT at each membrane potential by two-way repeated measures ANOVA with Tukey's post hoc test. (D) Summary  $I_K$  IV curves for the difference current between B and C, which is a measure of  $I_{to}$ .  $P = 0.85$  for  $I_{to}$  density between the WT and Akita by two-way repeated measures ANOVA. For B–D,  $n = 19$  WT and  $16$  Akita right atrial myocytes. (E) Representative  $I_K$  recordings at  $+30$  mV illustrating the effects of 4-AP ( $100 \mu\text{M}$ ), which inhibits  $K_v1.5$ -mediated  $I_K$ , in right atrial myocytes from WT and Akita mice. (F) Summary data illustrating the amplitude of the 4-AP-sensitive  $I_K$  in right atrial myocytes from WT and Akita mice.  $n = 9$  WT and  $10$  Akita right atrial myocytes. \* $P < 0.05$  vs. the WT by Student's  $t$  test. Current densities are measured in picoamperes/picofarad (pA/pF).

atrial electrical function is also affected by connexins, we measured the expression of *GJA5* and *GJA1* mRNAs, which encode Cx40 and Cx43, in the right atrium. *GJA5* and *GJA1* expressions were not altered in Akita mice (SI Appendix, Fig. S15).

Increases in APD could lead to the occurrence of triggered activity in the form of early afterdepolarizations (EADs). To assess this possibility, APs were measured at different pacing frequencies at baseline and in the presence of isoproterenol ( $1 \mu\text{M}$ ). No EADs were observed in wild-type or Akita right atrial myocytes in these studies (SI Appendix, Fig. S16).

**Effects of Chronic and Acute Insulin Treatment on Atrial Myocyte Electrophysiology in Akita Mice.** To investigate the basis for the beneficial effects of insulin on AF susceptibility and atrial conduction, we next examined the effects of chronic insulin treatment on atrial myocyte AP morphology (Fig. 7A). AP  $V_{\text{max}}$  was substantially increased following insulin treatment in Akita mice (Fig. 7B). In contrast, insulin treatment had no effect on action potential duration measured at 50% repolarization (APD<sub>50</sub>), action potential duration measured at 70% repolarization (APD<sub>70</sub>), or action potential duration measured at 90% repolarization (APD<sub>90</sub>) compared with placebo controls (Fig. 7C and SI Appendix, Table S14) so that APD remained prolonged in treated Akita mice (compare with wild-type values in Fig. 4).

Next, we measured right atrial  $I_{\text{Na}}$  in Akita mice treated chronically with insulin or placebo (Fig. 7D). Summary IV curves demonstrate that atrial  $I_{\text{Na}}$  was increased in Akita mice following chronic insulin treatment (Fig. 7E). Furthermore,  $I_{\text{Na}}$  activation curves (Fig. 7F) and kinetic analysis (SI Appendix, Table S13) demonstrate that chronic insulin increased  $I_{\text{Na}}$  in association with an increase in  $G_{\text{max}}$ , but there were no differences in  $V_{1/2(\text{act})}$  or slope factor. Western blot studies (Fig. 7G) illustrate that chronic insulin treatment increased the levels of  $\text{Na}_v1.5$  in the atria in Akita mice.

Consistent with the lack of effect of insulin on atrial APD, insulin treatment had no effect on  $I_K$  (with or without an inactivating prepulse) in Akita mice (SI Appendix, Fig. S17). Furthermore, chronic insulin treatment did not affect  $K_v1.5$  protein levels in Akita mice compared with placebo-treated controls (SI Appendix, Fig. S18).

We next sought to assess the effects of enhancing insulin signaling acutely (i.e., intraperitoneal injection of insulin) in Akita mice. Immediately following the reduction in blood glucose from acute insulin injection, right atrial myocytes were isolated, and AP morphology was assessed (Fig. 8A). Summary data illustrate that AP  $V_{\text{max}}$  was increased by acute insulin injection in Akita mice (Fig. 8B) but that APD<sub>50</sub>, APD<sub>70</sub>, and APD<sub>90</sub> were unaffected compared with saline controls (Fig. 8C and SI Appendix, Table S15). Notably, the increase in  $V_{\text{max}}$  was smaller after acute insulin compared with chronic insulin (SI Appendix, Fig. S19A).

Next, we measured  $I_{\text{Na}}$  in Akita right atrial myocytes isolated after acute insulin (or saline) injection (Fig. 8D).  $I_{\text{Na}}$  density was increased following acute insulin injection (Fig. 8E). This increase occurred in association with an increase in  $G_{\text{max}}$ , but there were no changes in  $V_{1/2(\text{act})}$  or slope factor (Fig. 8F and SI Appendix, Table S13) compared with saline controls. The increase in  $I_{\text{Na}}$  elicited by acute insulin was smaller than after chronic insulin (SI Appendix, Fig. S19B). Acute insulin injection had no effects on  $I_K$  in Akita atrial myocytes (SI Appendix, Fig. S20).

The role of acute insulin signaling was further investigated by dialyzing right atrial myocytes from Akita mice with PIP<sub>3</sub> [a direct mediator of insulin signaling downstream of the insulin receptor and PI3K (12, 14)] or PIP<sub>2</sub> (not a second messenger directly activated by insulin) as a control. Cells were dialyzed with these phospholipids ( $1 \mu\text{M}$ ) for 10 min, and then, atrial AP morphology was assessed (Fig. 8G). Summary data illustrate that PIP<sub>3</sub> increased  $V_{\text{max}}$  (Fig. 8H) to a similar extent as acute insulin (SI Appendix, Fig. S19A) but had no effects on APD (Fig. 8I and



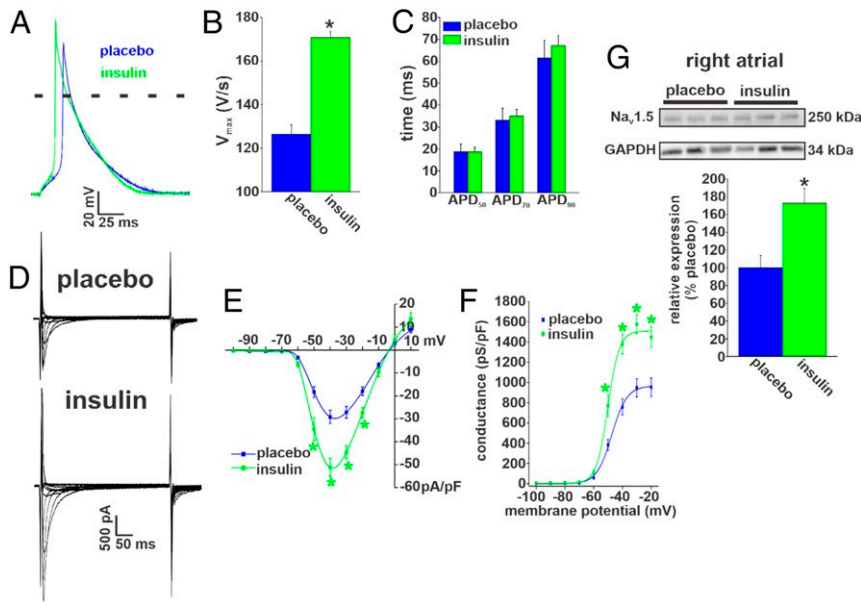


**Fig. 7.** Effects of chronic insulin treatment on atrial AP morphology and  $I_{Na}$  in Akita mice. (A) Representative right atrial APs in Akita mice treated with insulin or placebo for 4 wk. (B) Summary of the effects of chronic insulin on right atrial AP  $V_{max}$  in Akita mice. \* $P < 0.05$  vs. placebo by Student's  $t$  test. (C) Summary of the effects of chronic insulin on right atrial APD in Akita mice. Chronic insulin had no effect on APD compared with placebo. For AP measurements,  $n = 19$  myocytes for placebo and 14 for chronic insulin treatment. *SI Appendix, Table S14* has additional analysis of AP morphology. (D) Representative  $I_{Na}$  recordings in right atrial myocytes isolated from Akita mice treated chronically with insulin or placebo for 4 wk. Cell capacitances for these representative recordings were 31 pF for the wild type and 30 pF for Akita. (E) Summary  $I_{Na}$  IV curves for right atrial myocytes from Akita mice treated chronically with insulin or placebo. Current densities are measured in picoamperes/picofarad (pA/pF). (F) Summary  $I_{Na}$  activation curves for right atrial myocytes isolated from Akita mice treated chronically with insulin or placebo.  $n = 18$  myocytes for placebo and 13 myocytes for chronic insulin treatment. *SI Appendix, Table S13* has additional  $I_{Na}$  kinetic analysis. \* $P < 0.05$  vs. placebo by two-way repeated measures ANOVA with Tukey's post hoc test. Conductance is measured in picosiemens/picofarad (pS/pF). (G)  $Na_v1.5$  protein expression in the right atrium of Akita mice treated chronically with insulin or placebo.  $n = 6$  placebo-treated and 6 insulin-treated right atria. \* $P < 0.05$  vs. placebo by Student's  $t$  test.

*SI Appendix, Table S16*) compared with  $PIP_2$ -treated myocytes. Akita myocytes dialyzed with  $PIP_2$  were very similar to untreated Akita atrial myocytes (compare with Fig. 4).

Consistent with its effects on  $V_{max}$ ,  $PIP_3$  also increased atrial  $I_{Na}$  density in comparison with cells dialyzed with  $PIP_2$  (Fig. 8 *J* and *K*). This increase in  $I_{Na}$  was also similar to that seen following acute insulin treatment (*SI Appendix, Fig. S19B*). In addition,  $PIP_3$  increased  $I_{Na}$   $G_{max}$  without affecting  $V_{1/2(act)}$  or slope factor in Akita atrial myocytes (Fig. 8*L* and *SI Appendix, Table S13*).  $PIP_3$  had no effect on  $I_K$  in Akita atrial myocytes (*SI Appendix, Fig. S21*). Collectively, these data demonstrate that acutely enhancing insulin signaling selectively increases AP  $V_{max}$  and  $I_{Na}$  density in Akita atrial myocytes via  $PIP_3$  signaling without affecting APD or repolarizing  $I_K$ .

#### Protein Kinase C Inhibition Increases $I_{Na}$ in Akita Atrial Myocytes.

The data above demonstrate that enhancing insulin signaling increased atrial  $I_{Na}$  in Akita mice. These effects of insulin occurred without changes in  $V_{1/2(act)}$ ; however, our data also demonstrate that the reduction in  $I_{Na}$  in Akita mice is associated with a modest but significant shift in  $V_{1/2(act)}$  (*SI Appendix, Table S13*). It has been shown that protein kinase C (PKC) is elevated in the hearts of Akita mice (28), and PKC is a well-known modulator of the biophysical properties of  $I_{Na}$  (29). Accordingly, we tested the hypothesis that elevated PKC contributes to the reduction in atrial  $I_{Na}$  by dialyzing right atrial myocytes from Akita mice with the PKC inhibitor bisindolylmaleimide 1 (30) (BIM1; 1  $\mu$ M) (*SI Appendix, Fig. S22*). Compared with untreated Akita atrial myocytes, BIM1 increased  $I_{Na}$  density in Akita atrial myocytes (*SI Appendix, Fig. S22B*). Furthermore,  $I_{Na}$  activation curves (*SI Appendix, Fig. S22C*) and kinetic analysis (*SI Appendix, Table S13*) illustrate that BIM1 application increased  $I_{Na}$   $G_{max}$  and elicited a left shift in the  $V_{1/2(act)}$ . BIM1 also tended to reduce

the slope factor on the activation curve (*SI Appendix, Table S13*). These findings indicate that enhanced PKC activity in the atria of Akita mice contributes to the reduction in  $I_{Na}$  in association with a shift in  $I_{Na}$  activation kinetics.

#### Discussion

The present study demonstrates that, consistent with the human diabetic population (3, 5, 7), Akita and STZ-injected mice are highly susceptible to induced AF and that, when it occurred, AF was longer lasting in type 1 diabetic mice compared with wild-type controls. The increase in AF burden was associated with a prolongation of P-wave duration in Akita and STZ-injected mice, indicating that AF in type 1 DM is associated with impaired atrial electrical conduction. Akita and STZ-injected mice are well-established models of nonobese type 1 DM that are known to recapitulate many of the complications that occur in human DM (19, 31). Our observation that Akita and STZ mice also display increased susceptibility to AF establishes that these mice are excellent models of human type 1 DM that can be used for studying the relationships between DM and AF.

In further support of atrial electrical remodeling, we found that atrial AP morphology was substantially altered in Akita mice due to a reduction in  $V_{max}$  and increases in APD in association with reductions in atrial  $I_{Na}$  and  $I_{Kur}$ . While APD was also prolonged in ventricular myocytes in Akita mice, ventricular  $V_{max}$  was not significantly altered, suggesting that the reduction in  $V_{max}$  (and hence, the underlying  $I_{Na}$ ) in Akita mice may be restricted to the atria. On the other hand, a previous study did report a reduction in ventricular  $I_{Na}$  in type 1 diabetic rabbits (alloxan induced) (32). A prior study also demonstrated that ventricular APD is prolonged in Akita mice due, at least in part, to an increase in  $I_{Na,L}$  (33), whereas we did not observe any changes in  $I_{Na,L}$  in Akita atrial myocytes. Prior studies have also

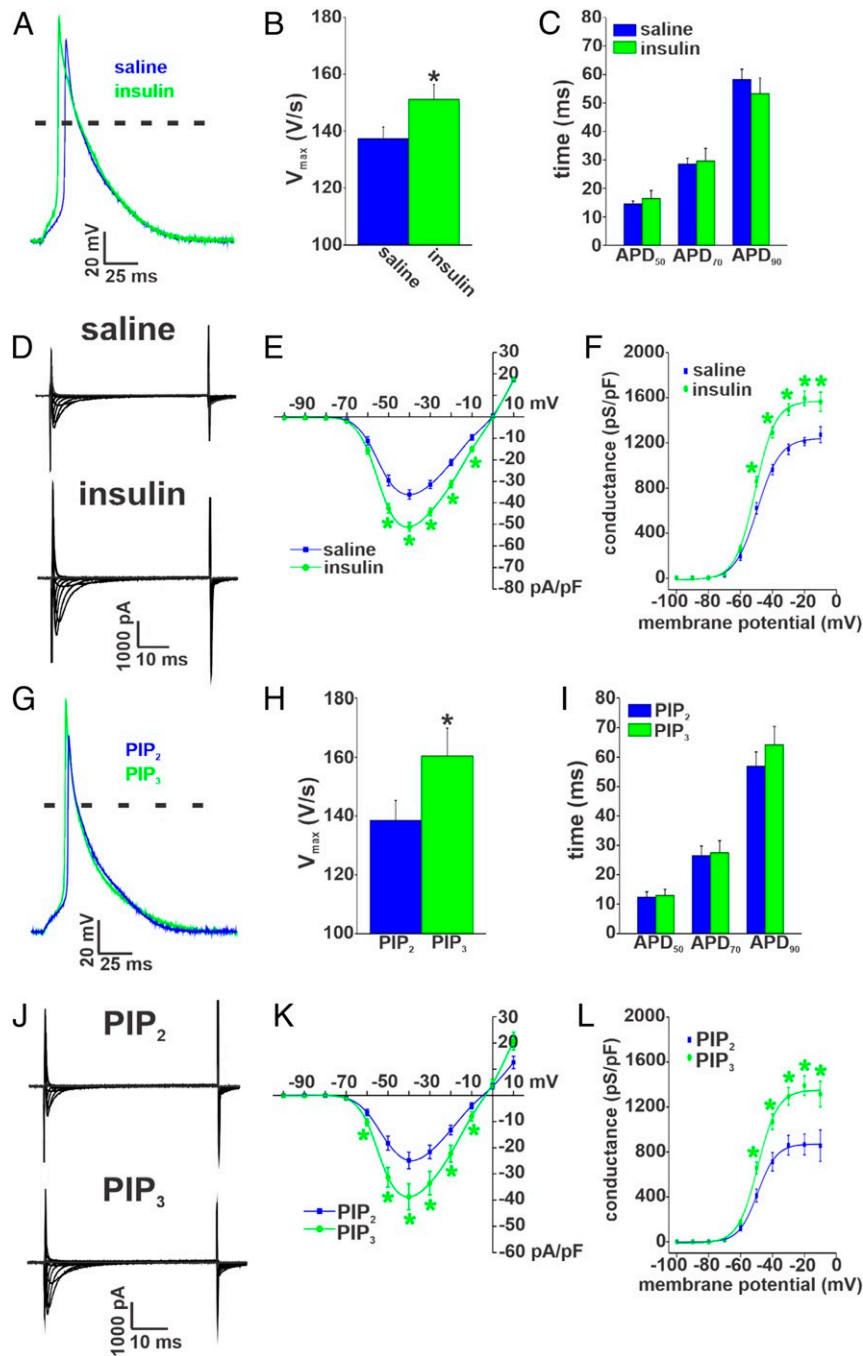


**Fig. 8.** Effects of acute insulin treatment and PIP<sub>3</sub> on atrial AP morphology and I<sub>Na</sub> in Akita mice. (A) Representative right atrial APs in Akita mice treated acutely with insulin or saline. (B) Summary of the effects of acute insulin on right atrial AP V<sub>max</sub> in Akita mice. \*P < 0.05 vs. saline by Student's t test. (C) Summary of the effects of acute insulin on right atrial APD in Akita mice. Acute insulin had no effect on right atrial APD compared with saline. For AP measurements, n = 14 myocytes for saline and 18 myocytes for acute insulin treatment. *SI Appendix, Table S15* has additional analysis of AP morphology. (D) Representative I<sub>Na</sub> recordings in right atrial myocytes isolated from Akita mice treated acutely with insulin or saline. Cell capacitances for these representative recordings were 42 pF for the wild type and 45 pF for Akita. (E) Summary I<sub>Na</sub> IV curves for right atrial myocytes from Akita mice treated acutely with insulin or saline. Current densities are measured in picoamperes/picofarad (pA/pF). (F) Summary I<sub>Na</sub> activation curves for right atrial myocytes isolated from Akita mice treated acutely with insulin or saline. n = 8 myocytes for saline and 12 myocytes for acute insulin treatment. *SI Appendix, Table S13* has additional analysis of I<sub>Na</sub> activation kinetics. \*P < 0.05 vs. saline at each membrane potential by two-way repeated measures ANOVA with Tukey's post hoc test. Conductance is measured in picosiemens/picofarad (pS/pF). (G) Representative APs in right atrial myocytes from Akita mice following dialysis with PIP<sub>3</sub> (1 μM) or PIP<sub>2</sub> (1 μM) as a control. Data are from cells dialyzed with phospholipids for 10 min. (H) Summary of the effects of PIP<sub>3</sub> on right atrial AP V<sub>max</sub> in Akita mice. \*P < 0.05 vs. PIP<sub>2</sub> by Student's t test. (I) Summary of the effects of PIP<sub>3</sub> on right atrial APD in Akita mice. PIP<sub>3</sub> had no effect on right atrial APD. For AP measurements, n = 7 myocytes for PIP<sub>2</sub> and 8 myocytes for PIP<sub>3</sub>. *SI Appendix, Table S16* has additional analysis of AP morphology. (J) Representative I<sub>Na</sub> recordings in right atrial myocytes from Akita mice following dialysis with PIP<sub>3</sub> (1 μM) or PIP<sub>2</sub> (1 μM) for 10 min. Cell capacitances for these representative recordings were 39 pF for the wild type and 38 pF for Akita. (K) Summary I<sub>Na</sub> IV curves for right atrial myocytes from Akita mice following dialysis with PIP<sub>3</sub> or PIP<sub>2</sub>. (L) Summary I<sub>Na</sub> activation curves for right atrial myocytes from Akita mice following dialysis with PIP<sub>3</sub> or PIP<sub>2</sub>. n = 10 myocytes for PIP<sub>2</sub> and 17 myocytes for PIP<sub>3</sub>. *SI Appendix, Table S13* has additional analysis of I<sub>Na</sub> activation kinetics. \*P < 0.05 vs. PIP<sub>2</sub> by two-way repeated measures ANOVA with Tukey's post hoc test.



demonstrated that  $I_{Ca,L}$  is reduced in ventricular myocytes in Akita mice (34) and PI3K $\alpha$  knockout mice (35) (an effect that would presumably lead to APD shortening), which is different from our observations in Akita atrial myocytes. Collectively, our study demonstrates that the changes in AP morphology (especially  $V_{max}$ ) and underlying ionic currents are different in the atria and ventricles in Akita mice and provides important insight into the distinct pattern of ion channel remodeling that occurs in the atria in Akita mice. Further work will be required to determine the basis for differences in atrial and ventricular electrophysiology in type 1 DM.

Chronic insulin treatment substantially reduced AF inducibility and burden and prevented changes in P-wave duration in Akita mice. Furthermore, acute application of insulin reduced the median duration of AF and shortened atrial P-wave duration. These findings suggest an important role for insulin signaling in the pathophysiology of AF in type 1 DM and indicate that this involves atrial electrical remodeling via both acute and chronic effects. In agreement with this, our studies also reveal a previously unknown role for insulin in regulating atrial  $I_{Na}$  in type 1 DM. We found that a major determinant of reduced  $I_{Na}$  in the atria of Akita mice was the reduction in atrial expression of *SCN5a* and *Nav1.5*. Chronic insulin treatment prevented the declines in atrial  $I_{Na}$  density and *Nav1.5* protein levels, indicating that insulin plays an important role in the de novo synthesis of new *Nav1.5* channels due to changes in gene expression. Consistent with this, previous studies have shown that activation of PI3K $\alpha$  up-regulates the expression of cardiac  $Na^+$  channels (36–38).

Importantly, our investigations revealed additional effects of insulin that could be activated acutely (i.e., on the order of minutes). Specifically, acute insulin injection immediately prior to cell isolation or dialysis of atrial myocytes with PIP $_3$  each increased atrial  $I_{Na}$  by ~30%. Consistent with these results, acute insulin also shortened P-wave duration. As these effects were rapid, we infer that they do not involve changes in gene or protein expression. Rather, these results demonstrate that an important component of the effects of insulin are mediated by the acute activation of PIP $_3$  signaling via PI3K.

In addition to the effects of insulin on atrial  $I_{Na}$ , we found that inhibition of PKC also increases atrial  $I_{Na}$  (~38%) in association with a shift in  $V_{1/2(act)}$  to values very similar to those measured in wild-type mice. This indicates that PKC activity is increased in the atria in Akita mice and that this can account for the change in  $I_{Na}$  activation kinetics. Consistent with this, PKC is known to be an important regulator of  $I_{Na}$  (29, 39), and previous studies have shown that PKC $\alpha$  expression is elevated in the heart in Akita mice (28). Thus, our studies demonstrate that atrial  $I_{Na}$  is reduced in Akita mice in association with both the loss of insulin signaling and enhanced PKC activity. The reductions in  $I_{Na}$  and AP  $V_{max}$  in the atria in Akita mice are likely major contributors to the increased susceptibility to AF in type 1 DM. These alterations can explain the impairments in atrial conduction and would be expected to be proarrhythmic by decreasing the wavelength of reentry (15, 40). This would favor of the occurrence and maintenance of AF and is consistent with AF being longer lasting in Akita mice.

Neither insulin or PIP $_3$  had any effect on the reduction in repolarizing  $I_K$  in Akita atrial myocytes, and APD remained prolonged. A reduction in *Kv1.5* is known to contribute to atrial electrical remodeling in human chronic AF (41), and our findings indicate this may be the case in Akita diabetic mice as well. Prolongation of the APD in Akita atrial myocytes could contribute to the increased susceptibility to AF by increasing the likelihood of triggered activity in the form of EADs (15); however, we did not observe EADs in our studies, suggesting that this is not a major determinant of AF in Akita mice. Consistent with this, our data demonstrate that chronic insulin treatment reduced

AF susceptibility and severity in association with improved atrial conduction,  $V_{max}$ , and  $I_{Na}$ , suggesting that these are critical for decreasing the inducibility of AF despite the lack of improvement in  $I_K$  or APD. Nevertheless, it is also possible that AP prolongation could contribute to impairments in atrial conduction in Akita mice either by contributing to the slowing of conduction at fast atrial rates or increasing the likelihood of conduction block. Additional studies will be required to determine how impaired atrial repolarization contributes to the slowing of atrial conduction and whether preventing AP prolongation can also reduce the susceptibility to AF in type 1 DM.

In addition to electrical remodeling, DM is also associated with structural remodeling due to atrial fibrosis. This has been demonstrated in human DM and in animal models (42–46). Indeed, we have previously demonstrated enhanced atrial fibrosis in the right and left atria in Akita mice (31). Fibrosis can also contribute to a substrate for AF since increased collagen deposition can impede atrial conduction and cause fragmentation of propagating wave fronts, thereby leading to reentry (15, 47–49). We have previously demonstrated that chronic insulin treatment reduces atrial fibrosis in Akita mice (31), and similar findings have been reported in STZ-injected rats treated with insulin (50). Thus, our prior work in combination with our present study demonstrates that insulin can prevent two alterations that are recognized as key contributors to impaired atrial conduction and maintenance of AF—the reduction in  $V_{max}$  due to reduced  $I_{Na}$  as well as increased atrial fibrosis—highlighting a previously unappreciated and important role for insulin as an antiarrhythmic agent for AF in type 1 DM. Consistent with these observations, it has been previously demonstrated that enhancing PI3K $\alpha$  (activated downstream of the insulin receptor) can mitigate ventricular electrical remodeling in hypertrophy and heart failure (51, 52) and that reduced PI3K $\alpha$  activity increases susceptibility to AF (53). Our data suggest that insulin must be delivered for timeframes that are adequate to increase the expression of *Nav1.5* and reduce fibrosis in order to maximize its protective effects on atrial electrical and structural remodeling in type 1 DM. While the acute activation of insulin signaling (PI3K/PIP $_3$  dependent) does increase atrial  $I_{Na}$ , and partially prevents P-wave prolongation, this was not sufficient by itself to fully reduce the AF burden or the prolongation in P-wave duration in vivo.

Some limitations of our study should be acknowledged. Our study was conducted in mice, which exhibit differences in the relative importance of some repolarizing  $I_K$  compared with humans. Specifically, the rapid and slow delayed rectifier  $K^+$  currents ( $I_{Kr}$  and  $I_{Ks}$ ), which are important in the human heart, do not play a major functional role in the mouse heart (18). Prior studies have shown alterations in some of these  $K^+$  currents in canine models of DM (54). Nevertheless, our study shows that  $I_{Kur}$  (carried by *Kv1.5* channels) is a major  $I_K$  that was altered in the atria in Akita mice. *Kv1.5* is an atrial-specific  $I_K$  in the human heart (18, 55). It will be insightful to explore the alterations that we have identified in large animal models, tissue samples from human diabetic patients, or possibly, stem cell-derived atrial myocytes. While our study has focused on key ion channels in the atria in type 1 DM, it is possible that there are other alterations in gene and protein expression that are sensitive to insulin regulation. This could be explored in future studies using RNA sequencing. While we did not observe any changes in the mRNA levels of atrial connexins, it is possible that other aspects of connexin function or regulation could be altered in the atria in type 1 diabetes. Similarly, we did not observe changes in atrial calcium transient morphology in Akita mice; however, other aspects of calcium homeostasis could be altered in type 1 diabetes, which could potentially play a role in triggering AF in diabetes: for example, by delayed afterdepolarizations. Based on our findings, it will be important to conduct further studies to examine the links between glycemic control,

atrial conduction patterns, and AF occurrence in human diabetic patients. Finally, it will also be important to explore the effects of insulin or of enhancing insulin signaling via PI3K and PIP<sub>3</sub> in type 2 DM to determine if similar alterations and effects are present in this condition.

In conclusion, our study provides mechanistic insight into the cellular and molecular basis for AF in type 1 DM. This work demonstrates that AF in this setting is associated with electrical remodeling and changes in AP morphology due to reductions in atrial I<sub>Na</sub> and K<sub>V</sub>1.5-mediated repolarizing I<sub>K</sub>. Furthermore, we have discovered that the reduction in I<sub>Na</sub> is multifactorial, involving distinct acute and chronic effects of insulin as well as enhanced PKC activity. Finally, we show that insulin treatment is antiarrhythmic in type 1 DM via effects on atrial Na<sup>+</sup> channels but not K<sup>+</sup> channels. These data indicate that AF in type 1 DM has distinct features associated with the loss of normal insulin signaling. These findings have important implications for the treatment of AF in type 1 diabetic patients.

## Materials and Methods

An expanded methods section is available in *SI Appendix*.

**Mice.** This study used male littermate wild-type and type 1 diabetic Akita mice between the ages of 16 and 22 wk. In some instances, male wild-type mice (16 to 18 wk) were treated with STZ (50 mg/kg intraperitoneal injection) to induce type 1 DM (56). The diabetic phenotype was confirmed by urinalysis to assess urine glucose (using keto-diastix reagent strips) as well as by measuring serum glucose levels (using a glucometer).

In chronic insulin treatment experiments, Akita mice were given insulin pellets (0.2 U/d per pellet) or placebo pellets (LinShin Canada Inc.) subcutaneously for 4 wk beginning at 12 wk of age. For acute insulin studies, Akita mice were given an intraperitoneal injection of insulin (5 to 10 U/kg) or saline, and 30 to 45 min later (after blood glucose was reduced), the mice were used experimentally.

All experimental procedures were approved by the University of Calgary Animal Care and Use Committee and the Dalhousie University Committee for Laboratory Animals and were in accordance with guidelines of the Canadian Council on Animal Care.

**Echocardiography and Electrolyte Measurements.** Cardiac structure and function were assessed by echocardiography in mice anesthetized by isoflurane inhalation (2%) using a Vevo 3100 ultrasound machine (Fujifilm VisualSonics) as we have described previously (21). Blood electrolytes were measured using an ePoc blood glass and electrolyte analyzer using blood samples drawn from the jugular vein.

**In Vivo Electrophysiology.** Surface electrocardiograms (ECGs) were measured in anesthetized mice (2% isoflurane inhalation) using 30-gauge subdermal needle electrodes (Grass Technologies). In conjunction, a 1.2F octapolar electrophysiology catheter (Transonic) was inserted into the right heart via an incision in the jugular vein and used to assess inducibility of AF during burst pacing as we have done previously (57, 58). Burst pacing protocols were standardized so that all mice were stimulated in identical fashion using the same pacing protocols. AF was defined as a rapid and irregular atrial rhythm (fibrillatory baseline in the ECG) with irregular R wave to R wave (RR) intervals lasting at least 1 s on the surface ECG and rapid irregular activity on the intracardiac atrial electrogram. AF was categorized into three groups: <5 s (brief), 5 to 30 s (nonsustained), and >30 s (sustained). Additional details are available in *SI Appendix*.

**High-Resolution Optical Mapping.** To study activation patterns and electrical conduction in the atria, high-resolution optical mapping was performed in isolated atrial preparations using methods that we have described in detail previously (31, 57, 59, 60). These atrial preparations were studied while in intrinsic sinus rhythm. Atrial preparations were immobilized using blebbistatin (10 μM) (61). Changes in fluorescence were captured using the voltage-sensitive dye Di-4-ANEPPS (10 μM) and a high-speed electron multiplying charge-coupled device camera at ~900 frames per 1 s. Spatial resolution was 67 × 67 μM per pixel. Conduction velocity was measured locally in the right and left atria using approaches described previously (21, 22, 57, 58). In some instances, optical APs were measured by measuring the change in fluorescence as a function of time at individual pixels in the right and left atria as previously described (21, 22). All experiments were performed at 35 °C. Data were analyzed using custom software written in Matlab. Further details are available in *SI Appendix*.

**Patch Clamping of Isolated Atrial Myocytes.** Right and left atrial myocytes were isolated from mice by enzymatic digestion as we have described previously (62, 63). These myocytes were used to record APs using the perforated patch-clamp technique or the whole-cell patch-clamp technique (so that compounds could be dialyzed into the cells). AP parameters analyzed include resting membrane potential, V<sub>max</sub>, overshoot, and APD. V<sub>max</sub> was measured as the maximum rate of rise of the AP potential (i.e., dV/dt<sub>max</sub>) between the resting membrane potential and the peak of the AP. I<sub>Na</sub>, I<sub>Na,L</sub>, I<sub>K</sub>, and I<sub>Ca,L</sub> were recorded using the whole-cell patch-clamp technique. The solutions and experimental protocols for each of these approaches are available in *SI Appendix*.

**qPCR.** Quantitative gene expression was measured in the right and left atria as we have previously described (21, 22). Intron-spanning primers for *SCN5a* (Na<sub>v</sub>1.5), *KCNA5* (K<sub>v</sub>1.5), *GJA5* (Cx40), and *GJA1* (Cx43) as well as glyceraldehyde 3-phosphate dehydrogenase (GAPDH) (reference gene) were used. Experimental protocols and primer sequences are in *SI Appendix*.

**Western Blotting.** For western blotting, right and left atrial samples were used to measure the protein expression of Na<sub>v</sub>1.5, K<sub>v</sub>4.2, K<sub>v</sub>4.3, and K<sub>v</sub>1.5 as well as GAPDH as the loading control. The procedures for these experiments are provided in *SI Appendix*.

**Calcium Transients.** Calcium transients were measured using confocal imaging in acutely isolated atrial myocytes. The solutions and experimental protocols are provided in *SI Appendix*.

**Statistical Analysis.** All data are presented as means ± SEM. Data were analyzed using Fisher's exact test, Student's *t* test, two-way ANOVA with Tukey's post hoc test, or two-way repeated measures ANOVA with Tukey's post hoc test as indicated in each figure. *P* < 0.05 was considered significant.

**Data Availability.** Relevant data and associated experimental protocols required for interpreting conclusions are included in the manuscript and the *SI Appendix*. Any additional information, data, or experimental reagents are available from the corresponding author upon request.

**ACKNOWLEDGMENTS.** This work was supported by Canadian Institutes of Health Research Operating Grants MOP 142486 and PJT 166105 (to R.A.R.). H.J.J. was the recipient of a Nova Scotia Graduate Scholarship and a Dalhousie Medical Research Foundation MacDonald Graduate Scholarship and holds a Killam Postdoctoral Fellowship. L.J.B. holds a Libin Cardiovascular Institute of Alberta Graduate Studentship. Y.L. holds a Canadian Institutes of Health Research Postdoctoral Fellowship. E.E.E. held a Heart and Stroke Foundation of Canada Fellowship. R.A.R. held a New Investigator Award from the Heart and Stroke Foundation of Canada.

- D. Dobrev, L. Carlsson, S. Nattel, Novel molecular targets for atrial fibrillation therapy. *Nat. Rev. Drug Discov.* **11**, 275–291 (2012).
- S. Nattel, B. Burstein, D. Dobrev, Atrial remodeling and atrial fibrillation: Mechanisms and implications. *Circ. Arrhythm. Electrophysiol.* **1**, 62–73 (2008).
- J. Andrade, P. Khairy, D. Dobrev, S. Nattel, The clinical profile and pathophysiology of atrial fibrillation: Relationships among clinical features, epidemiology, and mechanisms. *Circ. Res.* **114**, 1453–1468 (2014).
- S. Dahlqvist *et al.*, Risk of atrial fibrillation in people with type 1 diabetes compared with matched controls from the general population: A prospective case-control study. *Lancet Diabetes Endocrinol.* **5**, 799–807 (2017).
- Y. Lin *et al.*, Mechanism of and therapeutic strategy for atrial fibrillation associated with diabetes mellitus. *ScientificWorld J.* **2013**, 209428 (2013).
- A. R. Menezes *et al.*, Cardiometabolic risk factors and atrial fibrillation. *Rev. Cardiovasc. Med.* **14**, e73–e81 (2013).
- L. J. Bohne *et al.*, The association between diabetes mellitus and atrial fibrillation: Clinical and mechanistic insights. *Front. Physiol.* **10**, 135 (2019).
- Z. Xiong *et al.*, A machine learning aided systematic review and meta-analysis of the relative risk of atrial fibrillation in patients with diabetes mellitus. *Front. Physiol.* **9**, 835 (2018).
- S. Dublin *et al.*, Diabetes mellitus, glycemic control, and risk of atrial fibrillation. *J. Gen. Intern. Med.* **25**, 853–858 (2010).
- S. D. de Ferranti *et al.*, Type 1 diabetes mellitus and cardiovascular disease: A scientific statement from the American Heart Association and American Diabetes Association. *Circulation* **130**, 1110–1130 (2014).
- E. D. Abel, Insulin signaling in heart muscle: Lessons from genetically engineered mouse models. *Curr. Hypertens. Rep.* **6**, 416–423 (2004).
- G. Y. Oudit *et al.*, The role of phosphoinositide-3 kinase and pten in cardiovascular physiology and disease. *J. Mol. Cell. Cardiol.* **37**, 449–471 (2004).

13. B. Vanhaesebroeck, J. Guillermet-Guibert, M. Graupera, B. Bilanges, The emerging mechanisms of isoform-specific pi3k signalling. *Nat. Rev. Mol. Cell Biol.* **11**, 329–341 (2010).
14. B. Vanhaesebroeck, L. Stephens, P. Hawkins, Pi3k signalling: The path to discovery and understanding. *Nat. Rev. Mol. Cell Biol.* **13**, 195–203 (2012).
15. J. Heijman, N. Voigt, S. Nattel, D. Dobrev, Cellular and molecular electrophysiology of atrial fibrillation initiation, maintenance, and progression. *Circ. Res.* **114**, 1483–1499 (2014).
16. S. Nattel, Atrial electrophysiology and mechanisms of atrial fibrillation. *J. Cardiovasc. Pharmacol. Therapeut.* **8**(suppl. 1), S5–S11 (2003).
17. A. G. Kleber, Y. Rudy, Basic mechanisms of cardiac impulse propagation and associated arrhythmias. *Physiol. Rev.* **84**, 431–488 (2004).
18. J. M. Nerbonne, R. S. Kass, Molecular physiology of cardiac repolarization. *Physiol. Rev.* **85**, 1205–1253 (2005).
19. W. Hsueh *et al.*, Recipes for creating animal models of diabetic cardiovascular disease. *Circ. Res.* **100**, 1415–1427 (2007).
20. M. Yoshioka, T. Kayo, T. Ikeda, A. Koizumi, A novel locus, *mody4*, distal to *d7mit189* on chromosome 7 determines early-onset niddm in nonobese *c57bl/6* (Akita) mutant mice. *Diabetes* **46**, 887–894 (1997).
21. H. J. Jansen *et al.*, Distinct patterns of atrial electrical and structural remodeling in angiotensin II mediated atrial fibrillation. *J. Mol. Cell. Cardiol.* **124**, 12–25 (2018).
22. H. J. Jansen *et al.*, Npr-c (natriuretic peptide receptor-c) modulates the progression of angiotensin II-mediated atrial fibrillation and atrial remodeling in mice. *Circ. Arrhythm Electrophysiol.* **12**, e006863 (2019).
23. M. Mackasey *et al.*, Natriuretic peptide receptor-c protects against angiotensin II-mediated sinoatrial node disease in mice. *JACC Basic Transl. Sci.* **3**, 824–843 (2018).
24. H. Bugger *et al.*, Type 1 diabetic Akita mouse hearts are insulin sensitive but manifest structurally abnormal mitochondria that remain coupled despite increased uncoupling protein 3. *Diabetes* **57**, 2924–2932 (2008).
25. H. C. Kuo *et al.*, A defect in the Kv channel-interacting protein 2 (*kchip2*) gene leads to a complete loss of *i(to)* and confers susceptibility to ventricular tachycardia. *Cell* **107**, 801–813 (2001).
26. A. E. Lomax, C. S. Kondo, W. R. Giles, Comparison of time- and voltage-dependent K<sup>+</sup> currents in myocytes from left and right atria of adult mice. *Am. J. Physiol. Heart Circ. Physiol.* **285**, H1837–H1848 (2003).
27. C. Fiset, R. B. Clark, T. S. Larsen, W. R. Giles, A rapidly activating sustained K<sup>+</sup> current modulates repolarization and excitation-contraction coupling in adult mouse ventricle. *J. Physiol.* **504**, 557–563 (2001).
28. V. B. Patel *et al.*, Loss of angiotensin-converting enzyme-2 exacerbates diabetic cardiovascular complications and leads to systolic and vascular dysfunction: A critical role of the angiotensin II/at1 receptor axis. *Circ. Res.* **110**, 1322–1335 (2012).
29. C. Marionneau, H. Abriel, Regulation of the cardiac Na<sup>+</sup> channel *nav1.5* by post-translational modifications. *J. Mol. Cell. Cardiol.* **82**, 36–47 (2015).
30. D. Toullec *et al.*, The bisindolylmaleimide *gf 109203x* is a potent and selective inhibitor of protein kinase C. *J. Biol. Chem.* **266**, 15771–15781 (1991).
31. P. S. Krishnaswamy *et al.*, Altered parasympathetic nervous system regulation of the sinoatrial node in Akita diabetic mice. *J. Mol. Cell. Cardiol.* **82**, 125–135 (2015).
32. C. L. Stables *et al.*, Reduced Na<sup>(+)</sup> current density underlies impaired propagation in the diabetic rabbit ventricle. *J. Mol. Cell. Cardiol.* **69**, 24–31 (2014).
33. Z. Lu *et al.*, Increased persistent sodium current due to decreased pi3k signaling contributes to qt prolongation in the diabetic heart. *Diabetes* **62**, 4257–4265 (2013).
34. Z. Lu *et al.*, Decreased l-type Ca<sup>2+</sup> current in cardiac myocytes of type 1 diabetic Akita mice due to reduced phosphatidylinositol 3-kinase signaling. *Diabetes* **56**, 2780–2789 (2007).
35. Z. Lu *et al.*, Loss of cardiac phosphoinositide 3-kinase p110 alpha results in contractile dysfunction. *Circulation* **120**, 318–325 (2009).
36. L. M. Ballou, R. Z. Lin, I. S. Cohen, Control of cardiac repolarization by phosphoinositide 3-kinase signaling to ion channels. *Circ. Res.* **116**, 127–137 (2015).
37. K. Kaur *et al.*, Tgf-beta1, released by myofibroblasts, differentially regulates transcription and function of sodium and potassium channels in adult rat ventricular myocytes. *PLoS One* **8**, e55391 (2013).
38. K. C. Yang, Y. T. Tseng, J. M. Nerbonne, Exercise training and pi3kalpha-induced electrical remodeling is independent of cellular hypertrophy and AKT signaling. *J. Mol. Cell. Cardiol.* **53**, 532–541 (2012).
39. J. Brouillette, R. B. Clark, W. R. Giles, C. Fiset, Functional properties of K<sup>+</sup> currents in adult mouse ventricular myocytes. *J. Physiol.* **559**, 777–798 (2004).
40. S. Nattel, New ideas about atrial fibrillation 50 years on. *Nature* **415**, 219–226 (2002).
41. D. R. Van Wagoner *et al.*, Outward K<sup>+</sup> current densities and *kv1.5* expression are reduced in chronic human atrial fibrillation. *Circ. Res.* **80**, 772–781 (1997).
42. T. Kato *et al.*, Ages-rage system mediates atrial structural remodeling in the diabetic rat. *J. Cardiovasc. Electrophysiol.* **19**, 415–420 (2008).
43. T. Kato *et al.*, Angiotensin II type 1 receptor blocker attenuates diabetes-induced atrial structural remodeling. *J. Cardiol.* **58**, 131–136 (2011).
44. R. R. Lamberts *et al.*, Impaired relaxation despite upregulated calcium-handling protein atrial myocardium from type 2 diabetic patients with preserved ejection fraction. *Cardiovasc. Diabetol.* **13**, 72 (2014).
45. B. Li, Y. Pan, X. Li, Type 2 diabetes induces prolonged p-wave duration without left atrial enlargement. *J. Kor. Med. Sci.* **31**, 525–534 (2016).
46. M. Watanabe *et al.*, Conduction and refractory disorders in the diabetic atrium. *Am. J. Physiol. Heart Circ. Physiol.* **303**, H86–H95 (2012).
47. M. S. Dzeshka, G. Y. Lip, V. Snezhitskiy, E. Shantsila, Cardiac fibrosis in patients with atrial fibrillation: Mechanisms and clinical implications. *J. Am. Coll. Cardiol.* **66**, 943–959 (2015).
48. S. Rohr, Myofibroblasts in diseased hearts: New players in cardiac arrhythmias?. *Heart Rhythm* **6**, 848–856 (2009).
49. R. M. Wolf *et al.*, Atrial fibrillation and sinus node dysfunction in human ankyrin-b syndrome: A computational analysis. *Am. J. Physiol. Heart Circ. Physiol.* **304**, H1253–H1266 (2013).
50. S. Saito *et al.*, Glucose fluctuations increase the incidence of atrial fibrillation in diabetic rats. *Cardiovasc. Res.* **104**, 5–14 (2014).
51. K. C. Yang, P. Y. Jay, J. R. McMullen, J. M. Nerbonne, Enhanced cardiac pi3kalpha signalling mitigates arrhythmogenic electrical remodelling in pathological hypertrophy and heart failure. *Cardiovasc. Res.* **93**, 252–262 (2012).
52. K. C. Yang, Y. C. Ku, M. Lovett, J. M. Nerbonne, Combined deep microRNA and mRNA sequencing identifies protective transcriptomal signature of enhanced pi3kalpha signaling in cardiac hypertrophy. *J. Mol. Cell. Cardiol.* **53**, 101–112 (2012).
53. L. Pretorius *et al.*, Reduced phosphoinositide 3-kinase (p110alpha) activation increases the susceptibility to atrial fibrillation. *Am. J. Pathol.* **175**, 998–1009 (2009).
54. C. Lengyel *et al.*, Diabetes mellitus attenuates the repolarization reserve in mammalian heart. *Cardiovasc. Res.* **73**, 512–520 (2007).
55. D. Fedida *et al.*, *Kv1.5* is an important component of repolarizing K<sup>+</sup> current in canine atrial myocytes. *Circ. Res.* **93**, 744–751 (2003).
56. H. Bugger *et al.*, Genetic loss of insulin receptors worsens cardiac efficiency in diabetes. *J. Mol. Cell. Cardiol.* **52**, 1019–1026 (2012).
57. E. E. Egom *et al.*, Impaired sinoatrial node function and increased susceptibility to atrial fibrillation in mice lacking natriuretic peptide receptor c. *J. Physiol.* **593**, 1127–1146 (2015).
58. H. J. Jansen *et al.*, Atrial structure, function and arrhythmogenesis in aged and frail mice. *Sci. Rep.* **7**, 44336 (2017).
59. J. Azer, R. Hua, P. S. Krishnaswamy, R. A. Rose, Effects of natriuretic peptides on electrical conduction in the sinoatrial node and atrial myocardium of the heart. *J. Physiol.* **592**, 1025–1045 (2014).
60. M. Moghtadai *et al.*, The impacts of age and frailty on heart rate and sinoatrial node function. *J. Physiol.* **594**, 7105–7126 (2016).
61. V. V. Fedorov *et al.*, Application of blebbistatin as an excitation-contraction uncoupler for electrophysiologic study of rat and rabbit hearts. *Heart Rhythm* **4**, 619–626 (2007).
62. R. Hua *et al.*, Effects of wild-type and mutant forms of atrial natriuretic peptide on atrial electrophysiology and arrhythmogenesis. *Circ. Arrhythm Electrophysiol.* **8**, 1240–1254 (2015).
63. J. Springer *et al.*, The natriuretic peptides BNP and CNP increase heart rate and electrical conduction by stimulating ionic currents in the sinoatrial node and atrial myocardium following activation of guanylyl cyclase-linked natriuretic peptide receptors. *J. Mol. Cell. Cardiol.* **52**, 1122–1134 (2012).